3-1-2017

Multiple Exciton Generation in Si and Ge Nanocrystals: An ab Initio Comparative Study

Mahdi Gordi

Hamidrez Ramezani
The University of Texas Rio Grande Valley, hamidreza.ramezani@utrgv.edu

Mohammad Kazem Moravvej-Farshi

Recommended Citation

Gordi, Mahdi, Hamidreza Ramezani, and Mohammad Kazem Moravvej-Farshi. 2017. "Multiple Exciton Generation in Si and Ge Nanocrystals: An Ab Initio Comparative Study." The Journal of Physical Chemistry C 121 (11): 6374–79. https://doi.org/10.1021/acs.jpcc.7b00512.

Multiple Exciton Generation in Si and Ge Nanocrystals: An ab initio Comparative Study

Mahdi Gordi [†], *Hamidreza Ramezani* [‡], *and Mohammad Kazem Moravvej-Farshi* [†*]

[†] Faculty of Electrical and Computer Engineering, Advanced Devices Simulation Lab (ADSL), Tarbiat Modares University, P. O. Box 14115-194, Tehran 1411713116, Iran

[‡] Department of Physics, The University of Texas Rio Grande Valley, Brownsville, TX 78520, USA

Corresponding Author

*Email: moravvej@modares.ac.ir.

Phone: +98-21-82883367

Fax: +98-21-82884325

ABSTRACT

We have simulated multi-exciton generation (MEG) processes in Si and Ge nanocrystals, employing the equation of motion coupled cluster single and double as a high-level ab initio approach. Simulations, consistent with the experimental results reported so far, reveal the key role of the *d*-polarized valence component in the chosen basis set on the accuracy and reliability of the results. Moreover, the MEG thresholds calculated with def2SVP basis set are shown to be ~8.23(8.07) eV for seven (eight)-atom Si clusters and ~7.58(6.84) eV for similar Ge clusters. The normalized MEG thresholds of Ge nanocrystals are 8% smaller with respect to Si. Thus in contrast to Si, they are more appealing to the optical device designers for enhancing the device quantum efficiency. Furthermore, the resemblance of the symmetry of the simulated seven-atom clusters to those of the experimentally dome-like grown nanocrystals makes the behavior of their MEG quantum probability similar.

1. INTRODUCTION

Increasing the conversion efficiency of the light-harvesting devices is one of the most challenging issues facing the device design. In the ideal situation, an indirect single-junction solar cell reaches a conversion efficiency of 33% known as Shockley-Queisser limit.[1] This is obtained under the assumption of one electron-hole pair absorption by a single photon. The main portion of the energy of the absorbed photon is wasted through the phonon scattering and emission inside the device by heat conversion. Therefore, reduction of the energy loss is an approach in designing more efficient optical devices.[2]

Multiple exciton generation (MEG) can provide a great mechanism to increase the efficiency of an optical device. As a result, MEG has received an ample attention in recent years.[3-36] In a MEG process, several excitons are generated by the absorption of a single photon of energy greater than twice the semiconductor energy gap. If one can reduce the minimum required energy for MEG process to start in an optical device such as solar cell, the quantum efficiency increases accordingly. Nanocrystals are at the center of the attention because of their lower MEG thresholds with respect to the bulk semiconductors. They have unique optical properties that enhance the MEG process. There are several reasons for the improvement in the MEG process by nanocrystals. First, the physical dimension of a nanocrystal is close to the exciton Bohr radius. Consequently, the carriers' coulomb interaction becomes strong and therefore can improve the MEG process. Second, the large gaps between the energy levels of a nanocrystal can be greater than the optical phonon energy, causing the phonon bottleneck.[4,5] Moreover, the momentum conservation, which is a result of the crystal long-range periodic atomic potential, is relaxed in a zero-dimensional nanocrystal. Finally, the quantum confinement properties, such as shape, size, composition, and surface can influence the MEG process and increase the degree of

the freedom in the design of the MEG based devices.[6] The possibility of enhancing MEG by nanocrystals was first predicted by Nozik et al [4] and then approved experimentally for a number of nanocrystals, such a PbSe and PbS,[7-9] PbTe,[10] CdSe,[11,12] InAs,[13,14] Si,[15,16] and Ge.[17] In their prediction, Nozik et al [4] they also discussed about the effect of phonon bottleneck on the MEG enhancement. Despite the experimental confirmation of this effect by other research groups [18-20], there is still an on-going debate regarding this issue. For typically grown nanocrystals in which the upper states are degenerate and the energy separation between two adjacent levels is much smaller than the thermal energy (k_BT), thermal vibration of atoms lifts the degeneracy and relaxes the phonon bottleneck effect.[21-24] Selection rules, may not allow some of these states contribute to the optical transition. Nonetheless, the phonon-assisted relaxation between these states is highly probable. However, the role of phonon bottleneck in the lower states of these nanocrystals cannot be ignored. Moreover, in very small nanocrystals, wherein the carrier-carrier interaction is strong, the phonon bottleneck effect is pronounced.[25]

Experimental studies, so far, indicate that the MEG process is very fast (≤a few fs), and therefore its evolution cannot be followed. Three mechanisms have been proposed to explain MEG procedure in nanocrystals.[21] One of these mechanisms is claimed to be the incoherent coulomb scattering that plays a similar role in the impact ionization process in bulk semiconductors. This incoherent scattering can relax the hot carriers to the lower energy states that in turn excite the valence electrons across the bandgap, generating multiple e-h pairs [26,27]. Moreover, a photon of energy greater than twice the energy gap can form a coherent superposition of single and multiple excitons.[8] This photo-excited superposition state can be dephased via the coulomb interaction between their electronic population with phonons. The rate of this dephasing mechanism determines the MEG efficiency.[21,28-30] The last is the direct

mechanism, in which a multi-exciton state is strongly coupled to a virtual single exciton, as a consequence of which, multi-excitons can be generated instantaneously by an absorbed photon, via a perturbative process.[31,32] This mechanism, which is well-matched with our theoretical model used in this article, is independent of the phonon coupling. This explanation has been supported by the ultrafast time scale MEG experiments.[8,16]

Silicon (Si) and germanium (Ge) with unique properties are the key materials in optical devices, especially solar cells. Understanding of MEG in these materials can play a major role in the material selection or device design. Si and Ge with similar atomic structures and lattices have different intrinsic properties such as dielectric constant, energy bandgap, quantum confinement, and exciton binding energy. So, MEG is expected to be different in Si and Ge nanocrystals. A number of theoretical and experimental studies on MEG processes in Si nanocrystals have been reported in the literature,[15,16,33-35] so far, while there are only a couple of reports about MEG in Ge.[17,36] Unlike the single-particle-based DFT methods, multi-configurational *ab initio* approaches can accurately describe the multi-excitation states and hence the MEG process. In the previous *ab initio* studies,[34, 35] small basis sets like LANL2DZ [37] with symmetry adapted cluster configuration interaction (SAC-CI) method has been used. This has motivated us to investigate the effect of larger basis sets on the MEG. In this work, using the equation of motion coupled cluster single and double (EOM-CCSD) as a high-level *ab initio* approach, we have studied the MEG process in seven(eight)-atom Si and Ge nanocrystals (Si7(8) and Ge7(8)). In this comparative study, we have employed various basis sets up to def2-TZVP [38] (with 5S, 5P, 2D, 1F functional components) and obtained more accurate data. To the best of our knowledge, this is the first instance in which a comparative theoretical study of MEG processes in Si7(8) and Ge7(8) nanocrystals have been reported, to date.

2. COMPUTATIONAL METHODS

The EOM-CCSD method provides a useful path for extending the ground state, resulted from the CCSD model to the excited states.[39,40] In general, EOM-CCSD describes each excited state, $|\Psi_k\rangle$, as a superposition of all possible excitations from CCSD ground state $|\Psi_0\rangle$. This extension of the higher order excited configurations in the wave function depicts the dynamic electron correlation and the probability that multi-excitations are generated during the photo-excitation. By applying the linear excitation operator, $\hat{R}_k$, to $|\Psi_0\rangle$, we obtain:

$$|\Psi_k\rangle \equiv \hat{R}_k |\Psi_0\rangle = \hat{R}_k \, e^{(\hat{T})} |\Phi_{\mathrm{HF}}\rangle, \tag{1}$$

where $\hat{T}$ and $|\Phi_{\mathrm{HF}}\rangle$ are the coupled cluster excitation operator and the restricted Hartree-Fock reference determinant, and

$$\hat{R}_k = \hat{R}_{k,0} + \hat{R}_{k,1} + \hat{R}_{k,2} = r_0(k) + \sum_{a;i} r_i^a(k) \left\{ \hat{a}^\dagger \hat{i} \right\} + \frac{1}{4} \sum_{a,b;i,j} r_{ij}^{ab}(k) \left\{ \hat{a}^\dagger \hat{i} \hat{b}^\dagger \hat{j} \right\}, \tag{2}$$

in which $\hat{R}_{k;0}$, $\hat{R}_{k;1}$, and $\hat{R}_{k;2}$ are the reference, singly excited, and doubly excited components of the linear excitation operator. The subscripts *i* and *j*, represent the occupied states that can be annihilated by $\hat{i}$ and $\hat{j}$ and superscripts *a* and *b* correspond to the unoccupied states with $\hat{a}^\dagger$ and $\hat{b}^\dagger$ as the corresponding creation operators. Moreover, r_0, r_i^a, and r_{ij}^{ab} are the EOM amplitudes corresponding to the reference, single, and double excitation, respectively.

Quantum probability of observing a single (double) excitation in a photo-excited state equals the sum of the squares of the corresponding EOM amplitude (i.e. $\sum_{a;i} \left| r_i^a \right|^2$ or $\sum_{a,b;i,j} \left| r_{ij}^{ab} \right|^2$). One way to obtain the MEG quantum probability (efficiency) is to calculate the percentages of the

probabilities of the single and double excitations, that can be obtained by the reduced excitation level (REL),[41]

$$\mathrm{REL} = \frac{\sum_{n=0}^{2} n \left\langle \Phi \left| \left(R_{k,n}\right)^{\dagger} R_{k,n} \right| \Phi \right\rangle}{\sum_{n=0}^{2} \left\langle \Phi \left| \left(R_{k,n}\right)^{\dagger} R_{k,n} \right| \Phi \right\rangle} = \frac{\sum_{i,a} \left(r_a^i\right)^2 + 2 \sum_{i<j,a<b} \left(r_{ab}^{ij}\right)^2}{\left(r_0\right)^2 + \sum_{i,a} \left(r_a^i\right)^2 + \sum_{i<j,a<b} \left(r_{ab}^{ij}\right)^2} \tag{3}$$

in which $n = 0$, 1, 2 for reference, singly, and doubly excited components, respectively. The states configurations before and after absorption of a photon are different. Each configuration has a coefficient, denoting the contribution of that configuration to the electronic structure of the excited state. If the coefficient of the single excitation configuration is larger than that of the multi-excitation configuration, the single exciton generation is dominant. Therefore, the MEG probability (REL) is close to one. Otherwise, the MEG prevails.

This EOM-CCSD based calculation method is an advanced quantum methodology that includes electron correlation effects for both the ground and the excited states. In this approach, the static and dynamic properties of a photo-excited nanocrystal can be characterized by superposition states, and hence is much more accurate than the effective mass [8,42,43] and pseudo-potential[26,44] approaches. In this approach, unlike in the time domain methods (such as TDDFT), the time-dependent processes such as phonon-induced mechanisms cannot be considered. Nonetheless, it can precisely describe the initial photo-excitations that can be developed further by a number of mechanisms, including Auger processes, [45,26] phonon-induced dephasing, [28,29,46] and electron– phonon relaxing mechanisms.[22,47]

3. RESULTS AND DISCUSSION

Due to the computational cost of the EOM-CCSD, our simulations are limited to Si7(8) and Ge7(8) nanocrystals whose global structures are theoretically well established.[48,49] Using DFT

and B3PW91 functional with the def2-TZVP basis set in GAMESS-US [50] package, the nanocrystals have optimized in global minima in their neutral ground states. These have been successfully used in a variety of applications and shown to optimize the clusters geometry.[51] Our calculations show that under the same conditions the atomic structure of Si7(8) and Ge7(8) clusters are alike, similar to their bulk structures. Figure 1 shows the schematics of the globally optimized structures of these nanocrystals. The Si7 and Ge7 clusters have similar pentagonal bipyramid structures with D5h point group and Si8 and Ge8 are arranged in distorted bicapped octahedrons with C2h point group.

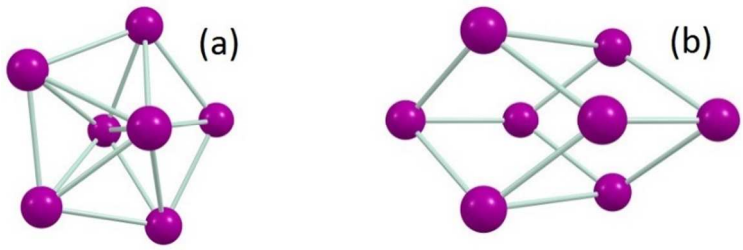

Figure 1. Schematics of (a) Si7 or Ge7 (b) Si8 or Ge8 nanocrystals optimized by global minima in their neutral ground states using DFT.

First, using various basis sets up to def2-TZVPD, we investigated the influence of the basis sets on the MEG threshold energy of the Si7. We also calculated the HOMO-LUMO and optical energy gaps (E_{HL} and E_{OP}) for Si7 and Ge7 clusters, as compared in Table 1. It is evident that use of the larger basis sets in the *ab initio* simulations should lead to the more accurate numerical data. Nonetheless, use of a very large basis set can be computationally prohibitive. The purpose of this study is to find a reasonable basis set that can lead to the numerical results with a reasonable accuracy. In doing so, we used def2-TZVPD (the largest basis sets among those shown in Table 1) as the reference basis set for our comparison.

Table 1. E_{HL} and E_{OP} for Si7 and Ge7, calculated for various basis sets [52] and related valence components.

Basis Set	Si7 cluster			Ge7 cluster		
	Valence Components	E_{HL} (eV)	E_{OP} (eV)	Valence Components	E_{HL} (eV)	E_{OP} (eV)
LANL2DZ*	2S, 2P	2.94	3.6	2S, 2P	2.65	3.48
LANL2DZdp	2S, 3P, 1D	2.68	3.30	2S, 3P, 1D	2.4	3.31
6-31G*	2S, 2P	2.88	3.57	2S, 2P, 1D	2.53	3.49
6-31G(d)	2S, 2P, 1D	2.69	3.39	2S, 2P, 2D	2.4	3.37
def2-SVP*	2S, 2P, 1D	2.71	3.36	2S, 2P, 2D	2.42	3.37
def2-SVPD*	2S, 2P, 2D	2.66	3.19	2S, 2P, 3D	2.39	3.29
def2-TZVP*	3S, 4P, 2D, 1F	2.65	3.16	4S, 4P, 4D, 1F	2.41	3.34
def2-TZVPD	4S, 4P, 3D, 1F	2.64	3.14	5S, 4P, 5D, 1F	2.39	3.29

* The basis set used for MEG quantum probability calculations.

The comparison shows that the E_{HL} and E_{OP} values obtained by LANL2DZ and 6-31G basis sets with no *d*-polarized valence components show the two largest deviations from those obtained by the reference basis set. Therefore, use of the basis sets with *d*-polarized valence components is crucial in these calculations. The optical bandgap of Si7 is smaller than that of Ge7, which is opposite to what we expect in the corresponding bulk structures. In all cases, the HOMO-LUMO gap of Ge7 is smaller than that of Si7.

Employing eq 3 we calculated the MEG quantum probability for Si7 cluster using the basis sets designated by asterisks in Table 1. In these calculations, only the valence orbitals in the active space are included. In addition, we used the largest abelian subgroup of D5h namely the C2V point group. The optical transitions from the ground state to the excited states in this point group are allowed only for A1, B1, and B2 symmetries. For each of these symmetries, we have considered at least hundred thirty lowest excited states. Figure 2 illustrates the quantum

probability of the MEG for the dark and bright states versus the normalized energy. The open symbols represent the data for the dark states, for which the oscillator strengths are near zero and the optical transition does not occur. The data for the bright states that contribute to the optical transitions are represented by the solid symbols. Comparison of the numerical results depicted in Figure 2a and 2b shows the MEG thresholds obtained by LANL2DZ or 6-31G basis sets with no *d*-polarized valence components are much smaller than that obtained by the reference basis set. Whereas, the MEG thresholds obtained by the three basis sets with *d*-polarized valence components, as compared on Figure 2b, are comparable.

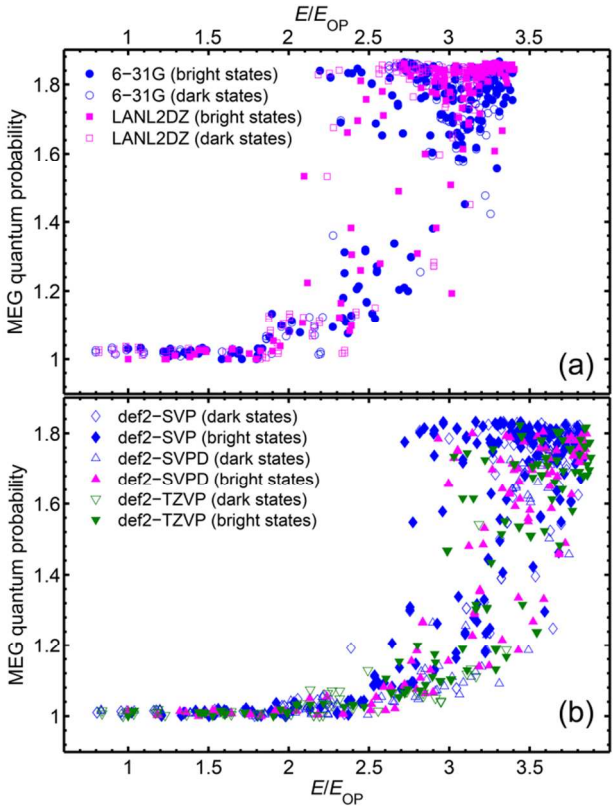

Figure 2. MEG quantum probability versus E/E_{OP} in Si7 cluster, using the basis sets (a) 6-31G and LANL2DZ; (b) def2-SVP and def2-SVPD, and def2-TZVP. The open and solid symbols

represent the dark and bright states, respectively. All data is normalized in terms of its optical energy gap.

The results for Si7 cluster obtained by LANL2DZ basis set is in agreement with the results obtained by others using the SAC-CI method.[34] The theoretical results on MEG in Si7 reported, so far,[34,35] are based on a basis set without *d*-polarized valence component, namely LANL2DZ. The calculated MEG quantum probabilities in these two reports were normalized with respect to the corresponding E_{HL} values and then compared with experimental results,[15] using the femtosecond transient absorption technique. However, to the calculated E_{HL} may not be included in optical transitions. To include all possible optical transition, in this work, we have calculated the MEG quantum probabilities versus the energy normalized with respect to E_{OP}, instead. As shown in Figure 2a, the MEG thresholds obtained by the smaller basis sets are smaller than $2\times E_{OP}$. This contradicts the energy conservation principle, indicating the vital role of the *d*-polarized valence component in the MEG quantum probability calculation. On the contrary, the MEG thresholds obtained from the three basis sets with the *d*-polarized valence component are about $E_{Th} \approx 2.4\times E_{OP}$, despite the differences in their optical energy gaps. This is in good agreement with the experimental results.[15] Henceforth, we use the def2-SVP, which is the smallest of the three basis sets.

Next, using def2-SVP we calculated the MEG quantum probability versus E/E_{OP} for the dark states (open symbols) and bright states (solid symbols) in Ge7 and compared the results with those of Si7, as shown in Figure 3. In order to relax the comparison, we also show the spline-smoothed data for the bright states by the solid curve and dashes-dots in this figure. The comparison shows that despite the similarity in the MEG quantum probability characteristics,

$E_{\text{Th-Si(Ge)7}} = 8.23(7.58)$ eV, or $E_{\text{Th-Ge7}}/E_{\text{OP-Ge7}} \approx 0.92\left(E_{\text{Th-Si7}}/E_{\text{OP-Si7}}\right)$. This means the MEG in Ge7 is ~8% stronger than that in Si7. This can be attributed to the slightly stronger quantum confinement in Ge nanocrystals.[53,54] Hence, the stronger the quantum confinement in nanocrystals, the more intense is the carriers' interaction, reducing the MEG threshold.

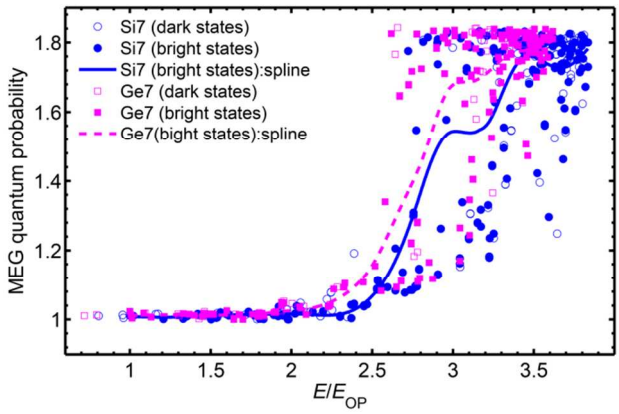

Figure 3. MEG quantum probability versus E/E_{OP} in Si7 and Ge7. The open and solid symbols represent the dark and bright states, respectively. The states energies are normalized in terms of its optical energy gap. The spline-smoothed data corresponding to the bright states are respectively depicted by the solid curve and dashes.

Employing def2-SVP basis set and using the C2h point group, we calculated the MEG quantum probability versus E/E_{OP} for the dark and bright states in Si8 and Ge8 nanocrystals, as shown by open and solid symbols in Figure 4. The allowed optical transitions from the ground state to excited states in the C2h point group follow Au and Bu symmetries. Our calculations show that the HOMO-LUMO and optical energy gaps for Si8 and Ge8 nanocrystals are $E_{\text{HL}} = 1.82$ and 1.59 eV and $E_{\text{OP}} = 2.60$ and 2.40 eV.

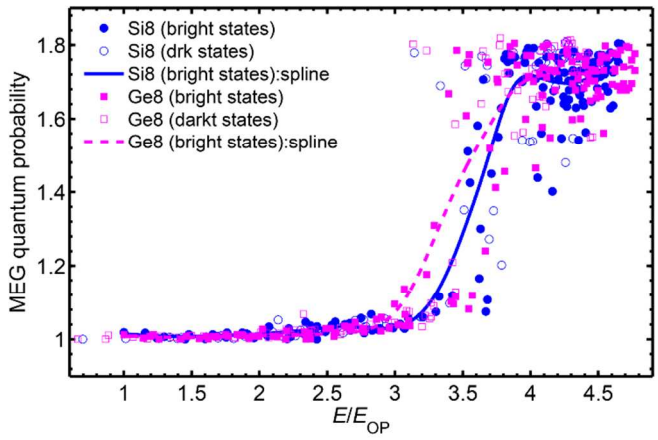

Figure 4. MEG quantum probability versus E/E_{OP} in Si8 and Ge8. The open and solid symbols represent the dark and bright states, respectively. The states energies are normalized in terms of its optical energy gap. The spline-smoothed data corresponding to the bright states are respectively depicted by the solid curve and dashes.

The MEG thresholds for Si8 and Ge8 nanocrystals extracted from the data shown in Figure 4 are respectively $E_{Th} = 8.07$ and 6.84 eV. Interestingly, the MEG threshold for the Ge8 normalized with respect to its optical energy gap is ~8% smaller than that of Si8 nanocrystal; the same as that obtained for their seven-atom counterparts — i.e., $E_{\text{Th-Ge8}}/E_{\text{OP-Ge8}} \approx 0.92\left(E_{\text{Th-Si8}}/E_{\text{OP-Si8}}\right)$. This could be generalized for the MEG thresholds for larger Ge and Si nanocrystals. It is noteworthy that this similarity is despite the significant difference in the relative shifts between the optical energy gaps of the seven-atom Si and Ge clusters as compared with the similar shift for their eight-atom counterparts. Moreover, comparison of Figure 4 with Figure 3 shows that the MEG quantum probabilities for the eight-atom clusters exhibit large shifts toward the higher normalized energies and their data are less scattered as compared with the seven-atom nanocrystals. These can be attributed to the lower symmetry of the eight-atom nanocrystals, with smaller optical gaps.

Finally, we compared the calculated MEG quantum probabilities for Si7(8) and Ge7(8) clusters with the data obtained from the experimentally grown nanocrystals made of Si (solid circles),[15] (solid triangles)[16] and Ge (solid squares),[17] as depicted in Figure 5.

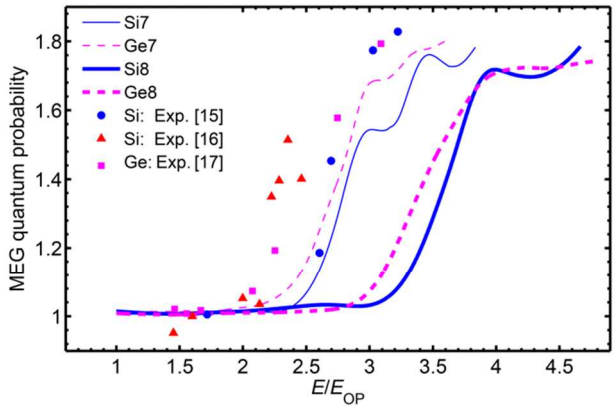

Figure 5. MEG quantum efficiency in Si nanocrystals: calculated for Si7 (tiny solid curve), Si8 (thick solid curve), and experimental data (solid circles [15]), and (solid triangles [16]); and calculate for Ge nanocrystals: Ge7 (tiny dashes), Ge8 (thick dashes) and experimental (solid squares [17]).

Our numerical results for Si7 and Ge7 are close to the experimental data for Si [15] and Ge [17]. This is due to the similarities in the Dh5 symmetry with the symmetries of the typically dome-like grown nanocrystals. On the contrary, the data obtained for the eight-atom clusters do not agree with those of the experiments. This might be due to the lower symmetry in eight-atom Si and Ge clusters. On the other hand, a significant difference in the two experimentally obtained MEG quantum probabilities for the Si clusters can be observed from Figure 5. This might be due to the different surface chemistries and hence different exciton relaxation dynamics for the nanocrystals, owing to the different conditions in which they were fabricated. The lack of enough experimental data on the Si and Ge nanocrystals and the inconsistency in the two sets of data on Si, reported so far, makes a fair comparison between their MEG processes difficult. Nonetheless, the numerical results reported in this paper show nearly similar behavior for the MEG quantum

probabilities for Si and Ge nanocrystals versus the energy normalized to their respective optical gaps.

4. SUMMARY AND CONCLUSION

Employing high-level *ab initio* approach we have calculated MEG quantum probabilities for Si and Ge nanocrystals versus energy normalized with their respective optical gaps. Simulations show that the calculated threshold energies for these clusters depend on the degree of the chosen basis sets. Specifically, the role of the *d*-polarized valence component of a basis set is vital in the results. The energy window over which single to multi-excitation transition takes place in the seven-atom Si(Ge) nanocrystal is wider than the transition window for the eight-atom Si(Ge) nanocrystal. This can be attributed to the larger degree of symmetry in the smaller cluster. The larger the degree of the symmetry, the larger the set of the selection rules, and hence the more transitions are available. Moreover, it is shown that the MEG threshold for Ge7(8) normalized with its optical gap is ~8% smaller than that of the Si7(8) nanocrystal. This can be generalized for the larger nanocrystals and hence makes the Ge nanocrystals more appealing for MEG processes for enhancing the quantum efficiency of the optical devices, such as solar cells and photo-detectors.

Corresponding Author

*Email: moravvej@modares.ac.ir.

Phone: +98-21-82883367

Fax: +98-21-82884325

Author Contributions

The authors declare no competing financial interest.

ACKNOWLEDGMENTS

H. R. gratefully acknowledges support from the UT system under the Valley STAR award.

REFERENCES

(1) Shockley, W.; Queisser, H. J. Detailed Balance limit of efficiency of P-N junction solar cells. *J. Appl. Phys.* **1961**, 32, 510.

(2) Hanna, M. C.; Nozik, A. J. Solar conversion efficiency of photovoltaic and photoelectrolysis cells with carrier multiplication absorbers. *J. Appl. Phys.* **2006**, 100, 074510.

(3) Beard, M. C. Multiple exciton generation in semiconductor quantum dots. *J. Phys. Chem. Lett.* **2011**, 2, 1282–1288.

(4) Nozik, A. J. Spectroscopy and hot electron relaxation dynamics in semiconductor quantum wells and quantum dots. *Annu. Rev. Phys. Chem.* **2001**, 52, 193-231.

(5) Nozik, A. J. Multiple exciton generation in semiconductor quantum dots. *Chem. Phys. Lett.* **2008**, 457, 115–120.

(6) Padilha, L. A.; Stewart, J. T.; Sandberg, R. L.; Bae, W. K.; Koh, W.; Pietryga, J. M.; Klimov, V. I. Carrier multiplication in semiconductor nanocrystals: influence of size, shape, and composition. *Acc. Chem. Res.* **2013**, 46, 1261–1269.

(7) Schaller, R. D.; Klimov, V. I. High efficiency carrier multiplication in PbSe nanocrystals: implications for solar energy conversion. *Phys. Rev. Lett.* **2004**, 92, 186601.

(8) Ellingson, R. J.; Beard, M. C.; Johnson, J. C.; Yu, P.; Mi´ci´c, O. I.; Nozik, A. J.; Shabaev, A.; Efros, A. L. Highly efficient multiple exciton generation in colloidal PbSe and PbS quantum dots. *Nano Lett.* **2005**, 5, 865-871.

(9) Cunningham, P. D.; Boercker, J. B.; Foos, E.; Lumb, M. P.; Smith, A. R.; Tischler, J. G.; Melinger, J. S. Enhanced multiple exciton generation in quasi-one-dimensional semiconductors. *Nano Lett.* **2011**, 11, 3476–3481.

(10) Murphy, J. E.; Beard, M. C.; Norman, A. G.; Ahrenkiel, S. P.; Johnson, J. C.; Yu, P.; Mi´ci´c, O. I.; Ellingson, R. J.; Nozik, A. J. PbTe colloidal nanocrystals: synthesis, characterization, and multiple exciton generation. *J. Am. Chem. Soc.* **2006**, 128, 3241-3247.

(11) Schaller, R. D.; Sykora, M.; Jeong, S.; Klimov, V. I. High-efficiency carrier multiplication and ultrafast charge separation in semiconductor nanocrystals studied via time-resolved photoluminescence. *J. Phys. Chem. B* **2006**, 110, 25332-25338.

(12) Nair, G.; Bawendi, M. Carrier multiplication yields of CdSe and CdTe nanocrystals by transient photoluminescence spectroscopy. *Phys. Rev. B* **2007**, 76, 081304.

(13) Aharoni, A.; Mokari, T.; Popov, I.; Banin, U. Synthesis of InAs/CdSe/ZnSe core/shell1/shell2 structures with bright and stable near-infrared fluorescence. *J. Am. Chem. Soc.* **2006**, 128, 257-264.

(14) Schaller, R. D.; Pietryga, J. M.; Klimov, V. I. Carrier multiplication in InAs nanocrystal quantum dots with an onset defined by the energy conservation limit. *Nano Lett.* **2007**, 7, 3469-3476.

(15) Beard, M. C.; Knutsen, K. P.; Yu, P.; Luther, J. M.; Song, Q.; Metzger, W. K.; Ellingson, R. J.; Nozik, A. J. Multiple exciton generation in colloidal silicon nanocrystals. *Nano Lett.* **2007**, 7, 2506-2512.

(16) Trinh, M. T.; Limpens, R.; de-Boer, W. D. A. M.; Schins, J. M.; Siebbeles, L. D. A.; Gregorkiewicz, T. Direct generation of multiple excitons in adjacent silicon nanocrystals revealed by induced absorption. *Nat. Photon.* **2012**, 6, 316–321.

(17) Saeed, S.; de-Weerd, C.; Stallinga, P.; Spoor, F. C.; Houtepen, A. J.; Siebbeles, L. D.; Gregorkiewicz, T. Carrier multiplication in germanium nanocrystals. *Light Sci. Appl.* **2015**, 4, e251.

(18) Geiregat, P.; Delerue, C.; Justo, Y.; Aerts, M.; Spoor, F.; Van Thourhout, D.; Siebbeles, L. D. A.; Allan, G.; Houtepen, A. J.; Hens, Z. A Phonon Scattering Bottleneck for Carrier Cooling in Lead Chalcogenide Nanocrystals. *ACS Nano* **2015**, 9, 778.

(19) Smith, C. T.; Tyrrell, E. J.; Leontiadou, M. A.; Miloszewski, J.; Walsh, T.; Cadirci, M.; Page, R.; O?Brien, P.; Binks, D.; Tomic, S. Energy structure of CdSe/CdTe type II colloidal quantum dots—Do phonon bottlenecks remain for thick shells? *Sol. Energ. Mat. Sol. Cells* **2016**, 158, 2, 160–167.

(20) Kumar, M.; Vezzoli, S.; Wang, Z.; Chaudhary, V.; Ramanujan, R. V.; Gurzadyan, G. G.; Bruno, A.; Soci, C. Hot exciton cooling and multiple exciton generation in PbSe quantum dots. *Phys. Chem. Chem. Phys.* **2016**, 18, 31107.

(21) Prezhdo, O. V. Multiple excitons and the electron–phonon bottleneck in semiconductor quantum dots: An ab initio perspective. *Chem. Phys. Lett.* **2008**, 1, 460.

(22) Kilina, S. V.; Kilin, D. S.; Prezhdo O. V. Breaking the Phonon Bottleneck in PbSe and CdSe Quantum Dots: Time-Domain Density Functional Theory of Charge Carrier Relaxation. *ACS Nano* **2009**, 3, 93–99.

(23) Schaller, R. D.; Pietryga, J. M.; Goupalov, S. V.; Petruska, M. A.; Ivanov, S. A.; Klimov, V. I. Breaking the Phonon Bottleneck in Semiconductor Nanocrystals via Multiphonon Emission Induced by Intrinsic Nonadiabatic Interactions. *Phys. Rev. Lett.* **2005**, 95, 196401.

(24) Cooney, R. R.; Sewall, S. L.; Anderson, K. E. H.; Dias, E. A.; Kambhampati, P. Breaking the Phonon Bottleneck for Holes in Semiconductor Quantum Dots. *Phys. Rev. Lett.* **2007**, 98, 177403.

(25) Pandey, A.; Guyot-Sionnest, P. Slow electron cooling in collodial quantum dots. *Science*, **2008**, 322, 929–932.

(26) Franceschetti, A.; An, J. M.; Zunger, A. Impact Ionization Can Explain Carrier Multiplication in PbSe Quantum Dots. *Nano Lett.* **2006**, 6, 2191–2195.

(27) Beard, M. C.; Midgett, A. G.; Hanna, M. C.; Luther, J. M.; Hughes, B. K.; Nozik, A. J. Comparing Multiple Exciton Generation in Quantum Dots to Impact Ionization in Bulk Semiconductors: Implications for Enhancement of Solar Energy Conversion. *Nano Lett.* **2010**, 10, 3019–3027.

(28) Kamisaka, H.; Kilina, S. V.; Yamashita, K.; Prezhdo, O. V. Ultrafast vibrationally-induced dephasing of electronic excitations in PbSe quantum dot. *Nano Lett.* **2006**, 6, 2295–2300.

(29) Madrid, A. B.; Kim, H.-D.; Habenicht, B. F.; Prezhdo, O. V. Phonon-Induced Dephasing of Excitons in Semiconductor Quantum Dots: Multiple Exciton Generation, Fission, and Luminescence. *ACS Nano* **2009**, 3, 2487–2494.

(30) Hyeon-Deuk, K.; Prezhdo, O. V. Time-Domain ab Initio Study of Auger and Phonon-Assisted Auger Processes in a Semiconductor Quantum Dot. *Nano Lett.* **2011**, 11, 1845–1850.

(31) Schaller, R.D.; Agranovich, V.M.; Klimov V.I. High-efficiency carrier multiplication through direct photogeneration of multi-excitons via virtual single-exciton states. *Nat. Phys.* **2005**, 1, 189.

(32) Isborn, C. M.; Kilina, S. V.; Li, X.; Prezhdo, O. V. Generation of Multiple Excitons in PbSe and CdSe Quantum Dots by Direct Photoexcitation: First-Principles Calculations on Small PbSe and CdSe Clusters. *J. Phys. Chem. C* **2008**, 11, 18291– 18294.

(33) Hyeon-Deuk, K.; Prezhdo, O. V. multiple exciton generation and recombination dynamics in small Si and CdSe quantum dots: an ab initio time-domain study. *ACS Nano* **2012**, 6, 1239–1250.

(34) Fischer, S. A.; Madrid, A. B.; Isborn, C. M.; Prezhdo, O. V. Multiple exciton generation in small Si clusters: a high-level, ab initio study. *J. Phys. Chem. Lett.* **2010**, 1, 232–237.

(35) Jaeger, H. M.; Fischer, S.; Prezhdo, O. V. The role of surface defects in multi-exciton generation of lead selenide and silicon semiconductor quantum dots. *J. Chem. Phys.* **2012**, 136, 064701.

(36) Vörös, M.; Wippermann, S.; Somogyi, B.; Gali, A.; Rocca, D.; Galli, G.; Zimanyi, G. T. Germanium nanoparticles with non-diamond core structures for solar energy conversion. *J. Mater. Chem. A* **2014**, 2, 9820-9827.

(37) Wadt, W. R.; Hay, P. J. Ab initio effective core potentials for molecular calculations. Potentials for main group elements Na to Bi. *J. Chem. Phys.* **1985**, 82, 284.

(38) Weigenda, F.; Ahlrichsb, R. Balanced basis sets of split valence, triple zeta valence and quadruple zeta valence quality for H to Rn: Design and assessment of accuracy. *Phys. Chem. Chem. Phys.* **2005**, 7, 3297-3305.

(39) Piecuch, P.; Kucharski, S. A.; Kowalski, K.; Musial, M. Efficient computer implementation of the renormalized coupled-cluster methods: The R-CCSD[T], R-CCSD(T), CR-CCSD[T], and CR-CCSD(T) approaches. *Comput. Phys. Commun.* **2002**, 149, 71-96.

(40) Kowalski, K.; Piecuch, P. New coupled-cluster methods with singles, doubles, and noniterative triples for high accuracy calculations of excited electronic states. *J. Chem. Phys.* **2004**, 120, 1715-1738.

(41) Wloch, M.; Gour, J. R.; Kowalski, K.; Piecuch, P. Extension of renormalized coupled-cluster methods including triple excitations to excited electronic states of open-shell molecules. *J. Chem. Phys.* **2005**, 122, 214107.

(42) Witzel, W. M.; Shabaev, A.; Hellberg, C. S.; Jacobs, V. L.; Efros A. L. Quantum simulation of multiple-exciton generation in a nanocrystal by a single photon. *Phys. Rev. Lett.* **2010**, 105, 137401.

(43) Zohar, G.; Baer, R.; Rabani, E. Multiexciton generation in IV-VI nanocrystals: The role of carrier effective mass, band mixing, and phonon emission. *J. Phys. Chem. Lett.* **2013**, 4, 317–322.

(44) Rabani, E.; Baer, R. Distribution of Multiexciton Generation Rates in CdSe and InAs Nanocrystals. *Nano Lett.* **2008**, 8, 4488–4492.

(45) Califano, M.; Zunger, A.; Franceschetti, A. Efficient inverse auger recombination at threshold in CdSe nanocrystals, *Nano Lett.* **2004**, 4, 525–531.

(46) Kamisaka, H.; Kilina, S. V.; Yamashita, K.; Prezhdo, O. V. Ab Initio Study of Temperature and Pressure Dependence of Energy and Phonon-Induced Dephasing of Electronic Excitations in CdSe and PbSe Quantum Dots. *J. Phys. Chem. C* **2008**, 112, 7800–7808.

(47) Prezhdo, O. V.; Photoinduced dynamics in semiconductor quantum dots: Insights from time-domain ab initiostudies. *Acc. Chem. Res.* **2009**, 42, 2005–2016.

(48) Zhu, X.; Zenga, X. C. Structures and stabilities of small silicon clusters: ab initio molecular-orbital calculations of Si7–Si11. *J. Chem. Phys.* **2003**, 118, 3558.

(49) Shvartsburg, A. A.; Liu, B.; Lu, Z.; Wang, C.; Jarrold, M. F.; Ho, K. Structures of germanium clusters: where the growth patterns of silicon and germanium clusters diverge. *Phys. Rev. Lett.* **1999**, 83, 2167-2170.

(50) Schmidt, M. W.; Baldridge, K. K.; Boatz, J. A.; Elbert, S. T.; Gordon, M. S.; Jensen, J. H.; Koseki, S.; Matsunaga, N.; Nguyen, K. A.; Su, S.; Windus, T. L.; Dupuis, M.; Montgomery, J. A. General atomic and molecular electronic structure system. *J. Comput. Chem.* **1993**, 14, 1347.

(51) Aguilera-Segura, S. M.; Seminario, J. M. Ab Initio Analysis of Silicon Nano-Clusters. *J. Phys. Chem. C* **2014**, 118, 1397–1406.

(52) https://bse.pnl.gov/bse/portal

(53) Bostedt, C.; Buuren, T. v.; Willey, T. M.; Franco, N.; Terminello, L. J. Strong quantum-confinement effects in the conduction band of germanium nanocrystals. *Appl. Phys. Lett.* **2004**, 84, 4056-4058.

(54) Kuo, Y.; Lee, Y. K.; Ge, Y.; Ren, S.; Roth, J. E.; Kamins, T. I.; Miller, D. A. B.; Harris, J. S. Strong quantum-confined Stark effect in germanium quantum-well structures on silicon. *Nature*, **2005**, 437, 1334-1336.

TOC Graphic

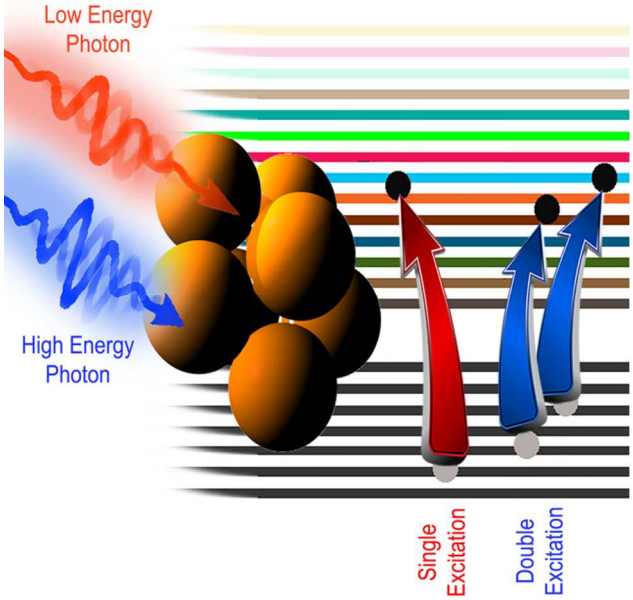
Low Energy
Photon
High Energy
Photon
Single
Excitation
Double
Excitation

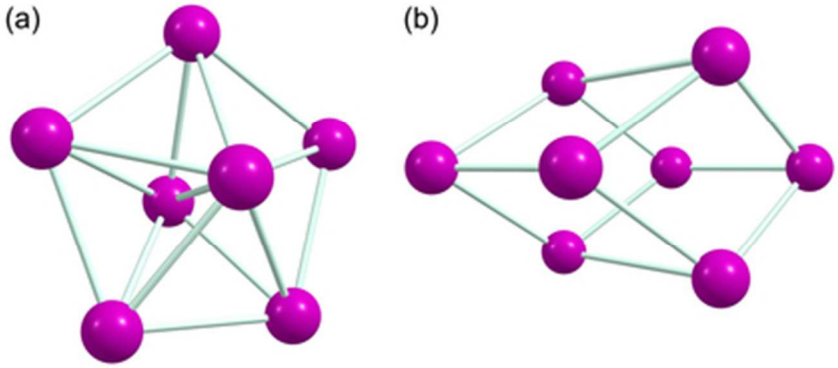

Schematics of (a) Si7 or Ge7 (b) Si8 or Ge8 nanocrystals optimized by global minima in their neutral ground states using DFT.

35x15mm (300 x 300 DPI)

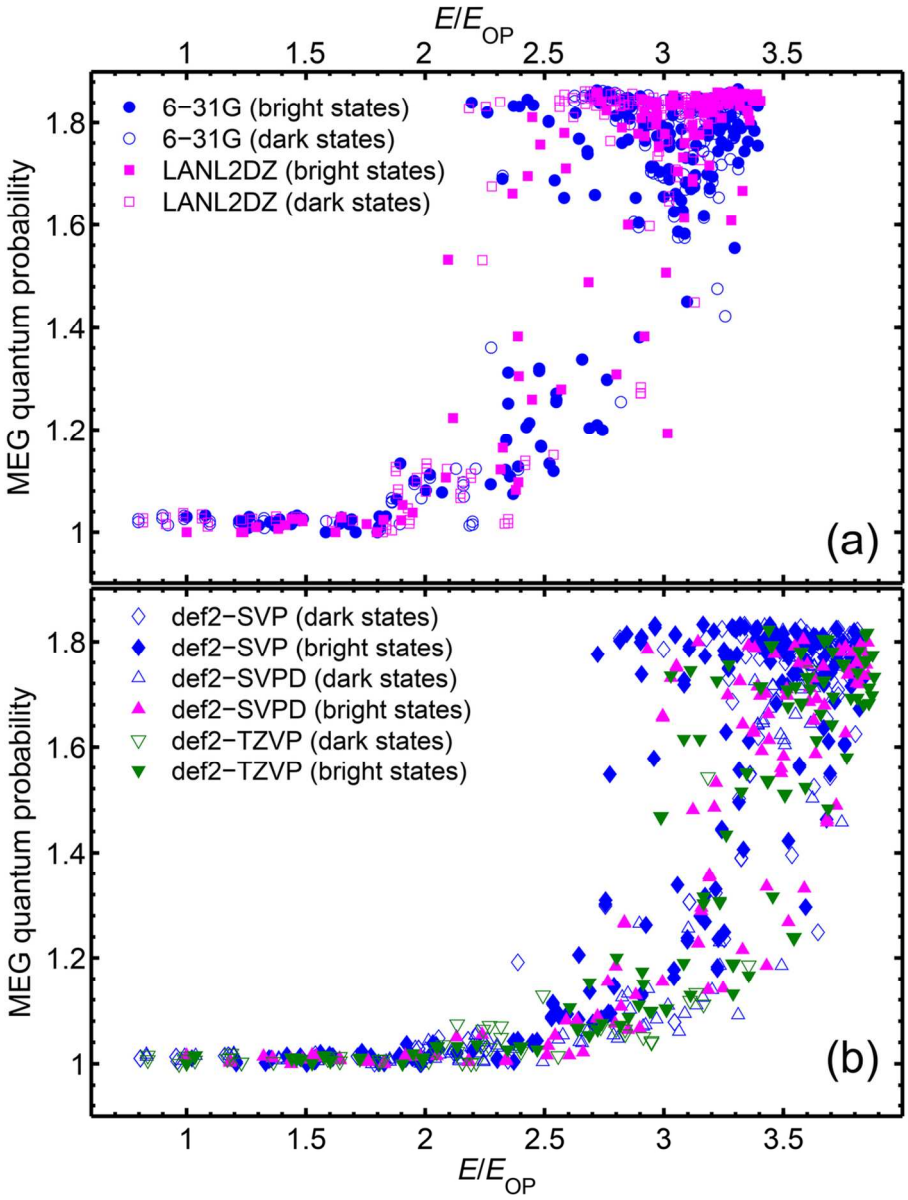

MEG quantum probability versus E/EOP in Si7 cluster, using the basis sets (a) 6-31G and LANL2DZ; (b) def2-SVP and def2-SVPD, and def2-TZVP. The open and solid symbols represent the dark and bright states, respectively. All data is normalized in terms of its optical energy gap.

106x137mm (300 x 300 DPI)

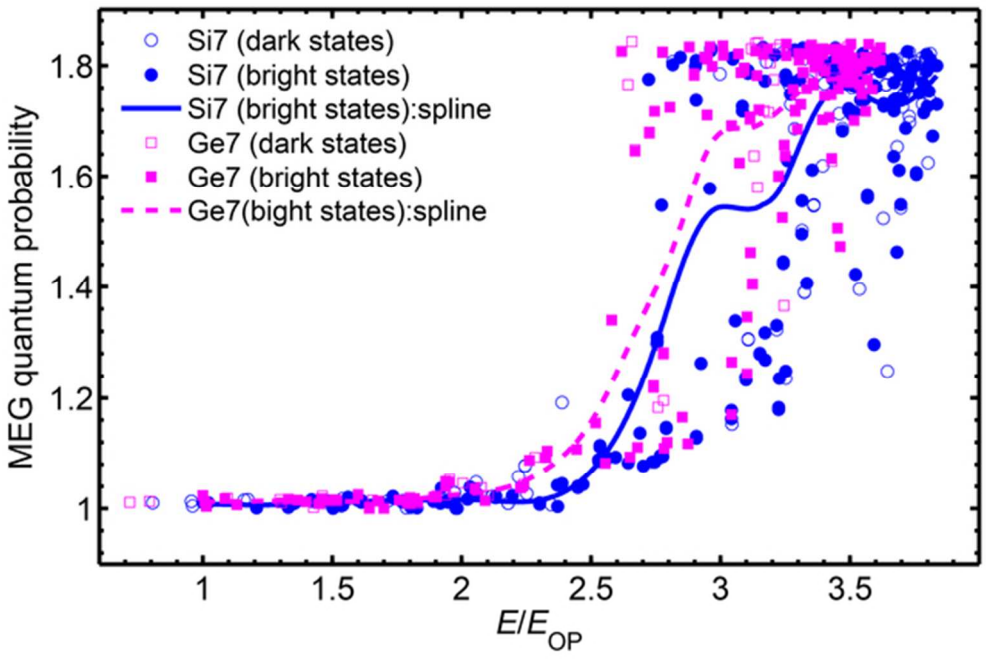

MEG quantum probability versus E/EOP in Si7 and Ge7. The open and solid symbols represent the dark and bright states, respectively. The states energies are normalized in terms of its optical energy gap. The spline-smoothed data corresponding to the bright states are respectively depicted by the solid curve and dashes.

55x36mm (300 x 300 DPI)

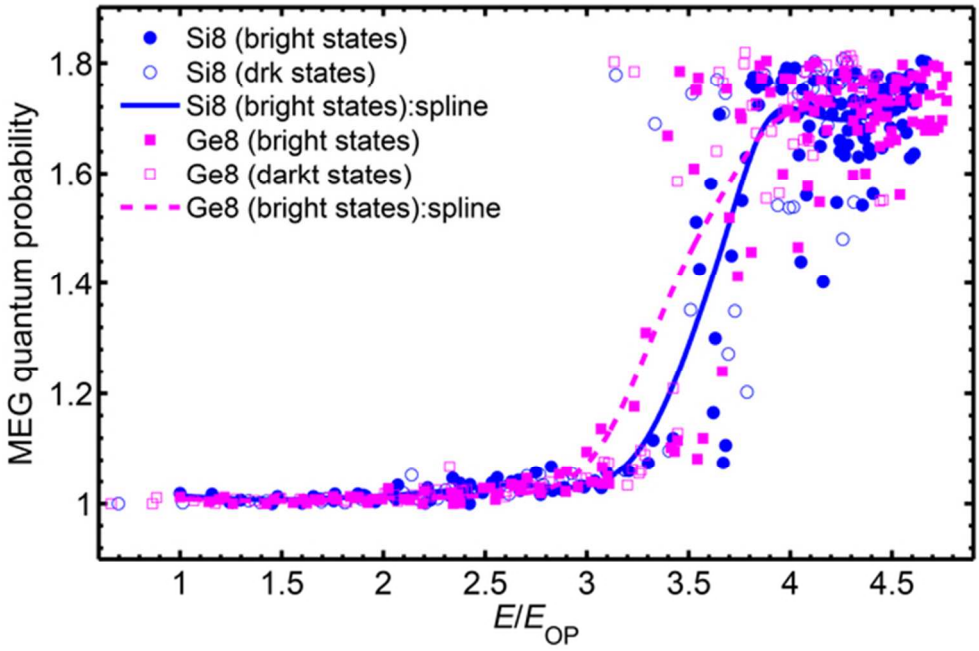

MEG quantum probability versus E/EOP in Si8 and Ge8. The open and solid symbols represent the dark and bright states, respectively. The states energies are normalized in terms of its optical energy gap. The spline-smoothed data corresponding to the bright states are respectively depicted by the solid curve and dashes.

55x36mm (300 x 300 DPI)

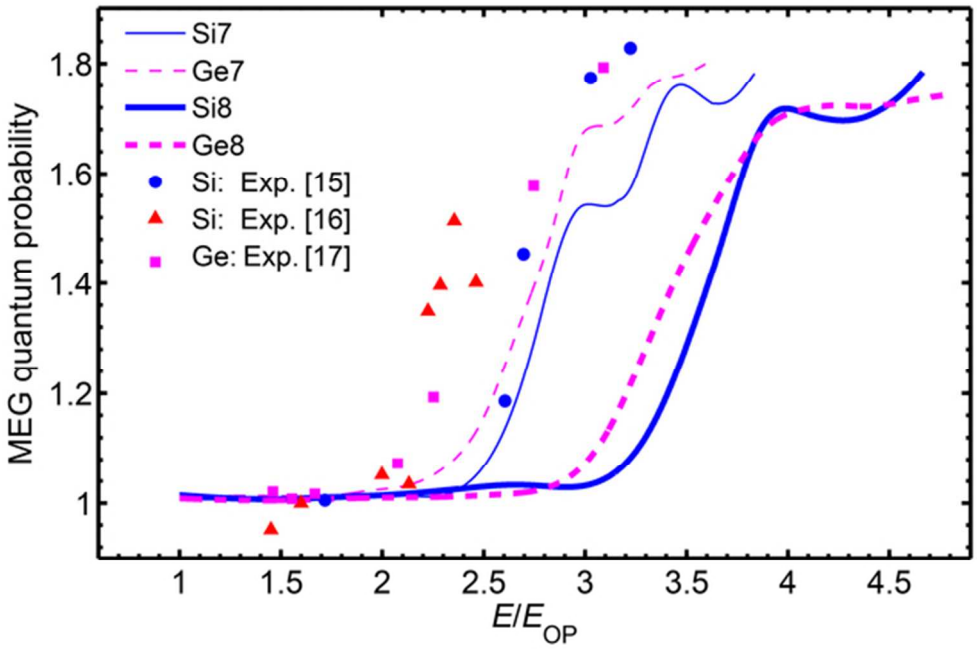

MEG quantum efficiency in Si nanocrystals: calculated for Si7 (tiny solid curve), Si8 (thick solid curve), and experimental data (solid circles 15), and (solid triangles 16); and calculate for Ge nanocrystals: Ge7 (tiny dashes), Ge8 (thick dashes) and experimental (solid squares 17).

55x36mm (300 x 300 DPI)

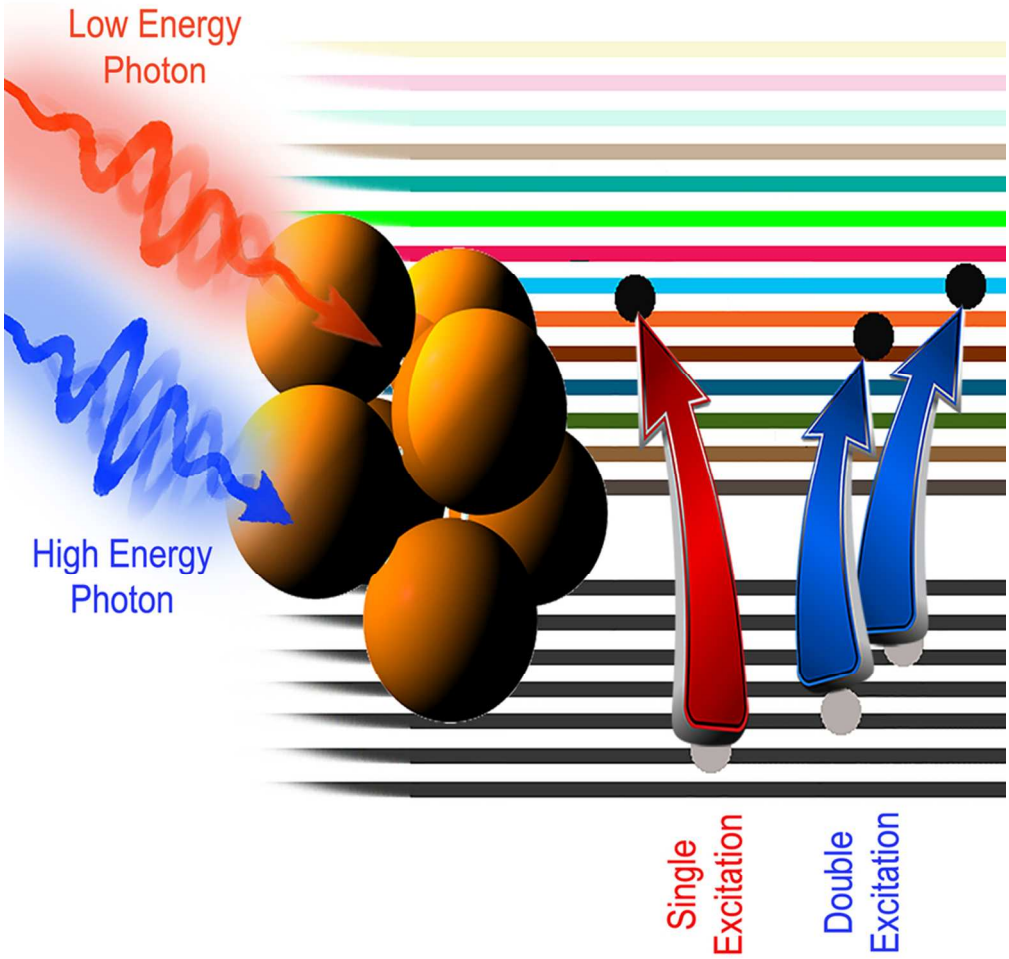

TOC Graphic

82x82mm (300 x 300 DPI)